Recovery of fatigue life using laser peening on 2024-T351 aluminium sheet containing scratch damage: The role of residual stress

Smyth, N., Toparli, M. B., Fitzpatrick, M. & Irving, P. E.

Recovery of fatigue life using laser peening on 2024-T351 aluminium sheet containing scratch damage: the role of residual stress

N Smyth[1,2], M B Toparli[3,4], M E Fitzpatrick[3,2], P E Irving[1a]

[1]School of Aerospace, Transport and Manufacturing, Cranfield University, Milton Keynes, MK43 0AL, UK
a Corresponding author
[2]Now at Faculty of Engineering, Environment & Computing, Coventry University, Priory Street, Coventry, CV1 5FB, UK
[3]Materials Engineering, The Open University, Walton Hall, Milton Keynes, MK7 6AA, UK
[4]Now at NORM R & D Centre, I.A.O.S.B., Cigli, Izmir, Turkey

ABSTRACT

The aim of the current work was to study the effect of laser shock peening (LSP) when applied to 2-mm-thick 2024-T351 aluminium samples containing scratch-like defects in the form of V-shaped scribes 50 – 150 μm deep. The scribes decreased fatigue life to 5% of that of the pristine material. The effect of laser peening on fatigue life was dependent on the specifics of the peen treatment, ranging from further reductions in life to restoration of the fatigue life to 61% of pristine material. Fatigue life was markedly sensitive to near-surface tensile residual stress, even if a compressive residual stress field was present at greater depth. Fatigue life after peening was also dependent on sample distortion generated during the peening process. Sample distortion modified local stresses generated by externally applied loads, producing additional life changes. Models based on residual stress intensity and crack closure concepts were successfully applied to predict fatigue life recovery.

Keywords

Laser Peening; Fatigue life recovery; Mechanical damage; Fatigue life prediction; Residual stress intensity

Nomenclature: K_t, elastic stress concentration factor; $K_{app\,max}$, Maximum externally applied stress intensity factor; $K_{app\,min}$, Minimum externally applied stress intensity factor; ΔK_{app}, externally applied stress intensity range; R, Ratio of applied stress intensity factors ($K_{app\,min}/K_{app\,max}$); K_{res}, Stress intensity factor due to residual stress field; $K_{tot\,max}$, Sum of external maximum stress intensity and stress intensity due to residual stress ($K_{tot\,max}=K_{app\,max}+K_{res}$); $K_{tot\,min}$, Sum of external minimum stress intensity and stress intensity due to residual stress ($K_{tot\,min}=K_{app\,min}+K_{res}$); ΔK_{eff}, effective stress intensity factor range for which the crack is open; R_{eff}, Effective R ratio for ΔK_{eff} load cycle; σ_{op}, stress in loading cycle at which the crack opens; σ_{max}, maximum stress in loading cycle; α, stress state at crack tip =1 for plane stress, 3 for plain strain; σ_o, Flow stress of material (mean of yield stress and ultimate tensile stress); A_o, A_1, A_2, A_3, Constants in Newman closure equations; σ_x, σ_y, Residual stresses in the X and Y directions; da/dN, crack growth rate; C,m,n, constants in the Walker Equation.

1 Introduction

Laser shock peening is a technique for the surface treatment of metallic materials. Laser peening improves fatigue performance of the treated component by creating a layer of compressive residual stress at the surface. It has been used extensively in the aerospace industry for the treatment of gas turbine blades and discs, and more recently wing attachment lugs[1]. There are two categories of LSP treatment[2,3]; one with relatively high energy per pulse (>10 J)and a large laser spot sizes (>3 mm). The other uses lower energies and smaller spot sizes.

Residual stress fields produced by laser peening have been measured for steel[4], titanium[5], and aluminium[6]. Most investigations have been on plates at least 5 mm thick and report substantial compressive residual stresses under the peen patch for the high energy process. In thin (1-3 mm) sheet 'over-peening'[7,8] needs to be avoided as this reduces near surface compressive stresses or

generates tensile stress[9], and lower energies are required. Eigenstrain approaches have proved useful in predicting residual stress fields in laser peened components as a function of geometry and of pre existing fields[9,10]. Finite element calculations[11,12] confirmed these observations and showed as sheet thickness increased from 3 to 6 mm, surface compressive stress on peened and unpeened faces of thin sheet was predicted[13] to decrease, and was actually greater on the unpeened side.

There is an emerging consensus on the roles of laser spot diameter, spot overlap, laser energy and laser spot raster pattern[3,12-15] in determining residual stress fields. Increasing laser energy, power density and coverage all increase the peak subsurface compressive residual stresses. Increasing spot diameter increases the depth of compression without changing the maximum. Many researchers have reported the residual stress component in the direction of the raster to be larger than the stress component perpendicular to it. Correa *et al.*[16] have demonstrated that a random pattern of laser spots produces a closer approximation to an equibiaxial field.

The fatigue response to laser peen residual stress fields show considerable variability, depending on sample thickness and peen patch configuration. Test configurations where cracks initiate at locations with balancing tensile residual stresses, report small positive or adverse effects on life. If the initiation site is within the compressive stress area then fatigue lives are improved significantly. For example in tests on samples with holes, Ivetic *et al.*[2] and Achintha *et al.*[17] found that the laser peen stress field obtained depended on sample thickness and on the relative order of peening and hole drilling operations. The eventual fatigue life obtained depended on whether initiation took place at regions of tensile or compressive residual stress, with only initiation at compressive residual stress fields giving significant improvements.

For situations where life is dominated by fatigue crack growth, it has been demonstrated that the fatigue crack growth rate reduction produced by laser peening is greatest for thin sheet and least for thick plate. Both crack acceleration and retardation have been reported depending on the sign of the residual stresses at the crack tip location. The behaviour was successfully modelled[3,7,18,19] using crack closure approaches.

Laser peening also has been used to recover fatigue life in FOD damaged samples[19]. The stress fields surrounding FOD damage in titanium and nickel base superalloys have been studied[20,21]. Laser peening prior to FOD impact is reported to reduce tensile residual stresses caused by FOD deformation by about 30%[19] with concomitant benefits to fatigue life.

To better understand the interaction between FOD and scratch indentation geometry and peen residual stress fields determining fatigue life recovery; in this research surface scribes were cut in aluminium sheet with a diamond tipped tool. A scribing technique, fully described in[22,23] was used. This minimised deformation and residual stresses due to cutting. The same scribing procedure was used successfully to create scratches free of deformation and residual stress in the work of Dorman *et al.*[3] and Cini *et al.*[22]. The effects of different scratch depths and of four different peening processes on fatigue lives and residual stress fields have been studied. A ΔK_{eff}-based fatigue life prediction model was developed, allowing predicted lives to be compared to experimental ones.

2 Materials and Methods

2.1 Material

The material used was 2-mm-thick 2024-T351 clad aluminium sheet. The clad layer was approximately 60 μm thick and of soft unalloyed 1080 aluminium, applied by a roll bonding process. The mechanical properties were obtained by tensile tests according to ASTM B557M. Test sample orientation was perpendicular to the sheet rolling direction. Mean test results from three duplicate tests were proof strength 310 MPa, tensile strength 420 MPa and elongation at fracture 15%.

2.2 Fatigue test sample design

Fatigue tests were conducted in tension-tension loading and used dogbone shaped samples as illustrated in Figure 1. The samples were 400 mm long with a minimum section width of 80 mm. Defects to initiate fatigue cracks were introduced by scribing the samples using a diamond tool with a tip radius of 5 μm[23]. The scribes were perpendicular to the loading direction across the minimum width section. Scribe depths were 50 and 150 μm ±3 μm across the width.

K_t values of 50 μm and 150 μm scribes were determined using FE analysis by Cini[22,23] and had values of 8 and 14 respectively. Cini & Irving[22] found in the 150 μm scribed samples that the fatigue life was just 5% of the life of pristine material.
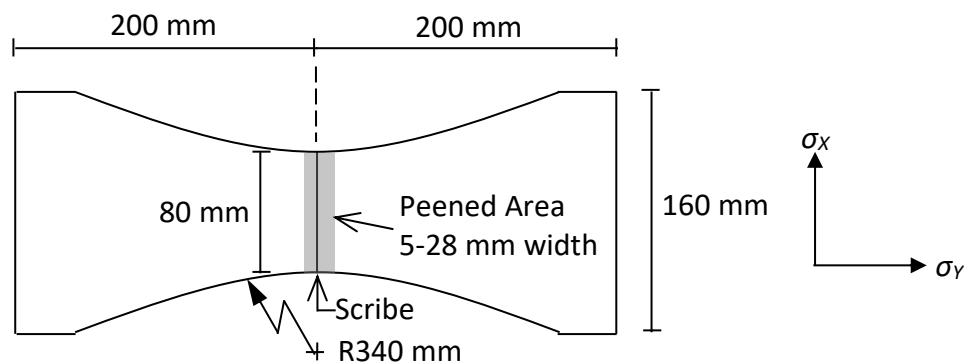

Figure 1: Schematic diagram of the dog-bone specimens used for tension-tension fatigue tests

2.3 Laser peening treatments

Laser peening was undertaken using three different peening systems. A total of four peening treatments were used and will be referred to as LSP-A, -B,-C and –D. The laser types and peen parameters are given in Table 1. Laser peening was applied to one side of the samples only, after first scribing them. All treatments had the laser tracking direction parallel to the scribe line and were applied across the entire 80 mm sample width.

Treatments LSP-A and LSP–B used the same peening parameters with a water jet tamping layer and aluminium foil ablative tape. LSP-A utilised a pattern of three peened rows, each offset by 30% as illustrated in Figure 2 (A). The total width of the treated area in the loading direction was ≈15 mm.

LSP-B was similar except it utilised a pattern of nine peened rows each offset by 30% the total width of the treated area was ≈28 mm as illustrated in Figure 2 (B).

Table 1: Comparison of laser peening parameters

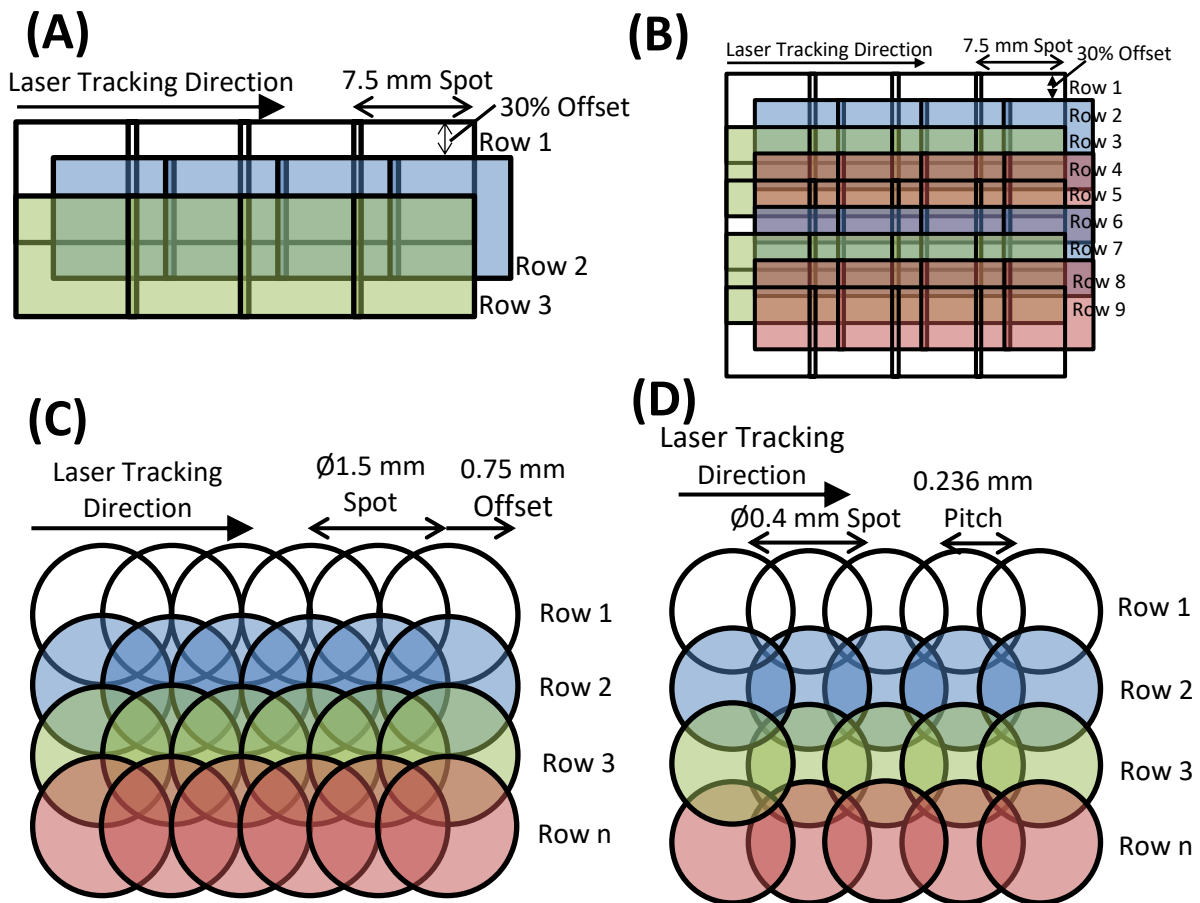| Treatment	LSP-A & -B	LSP-C	LSP-D
Laser type	Nd:YLF	Nd:YAG	Nd:YAG
Wavelength / nm	1064	1064	532
Laser spot geometry	Square	Circular	Circular
Laser spot diameter / mm	7.5	1.5	0.4
Laser pulse duration / ns	18	10	8
Energy per pulse / J	15.2	2.8	0.02
Power density / GW.cm^{-2}	1.5	15.72	1.99

Figure 2: (A) LSP-A peen pattern consisting of three laser peening layers, (B) LSP-B peen pattern consisting of nine laser peening layers, (C) LSP-C peening pattern and (D) LSP-D peening pattern

LSP-C used a water jet tamping layer and no ablative tape. The peening pattern is illustrated in Figure 2 (C). The treated area was approximately 5 mm wide with an overlapping pitch of 0.75 mm.

For LSP-D the specimens were submerged in a water bath without ablative tape. The treated area was approximately 5 mm wide, and the diameter of the laser spot was 0.4 mm. The offset pitch across the first 20mm was 0.136 mm (54 pulses per mm^2); across the central 40 mm it was 0.236 mm (18 pulses per mm^2); and across the remaining 20 mm it was 0.136 mm. The peening pattern is illustrated in Figure 2 (D).

2.4 Measurement of residual stress fields

Residual stress measurements were performed using incremental hole drilling on samples not intended for fatigue testing but subjected to identical peening treatment. Hole drilling was performed using a system supplied by Stresscraft Ltd and residual stress strain gauges of type Vishay CEA-13-062UL-120. The measurements were performed according to the guidance given in the NPL Good Practice Guide[24]. A hole of nominal diameter 2 mm was introduced by orbital hole milling and the final diameter of the hole after drilling was measured to an accuracy of 0.01 mm. Strain changes were recorded at depth increments of increasing size to a total hole depth of just over 1.4 mm. Strains from the three gauges were recorded for each depth increment.

The results were interpreted using the integral method developed by Schajer[25], with Stresscraft RS INT software version 5.1.2. The elastic properties used in the conversion from strain to stress of the aluminium were assumed to be E = 72 GPa and v = 0.33. Since the clad layer has the same modulus as the substrate alloy, the calculation of residual stress is unaffected by it.

A total drilled hole depth of 1.4 mm is not generally advisable for a sample 2 mm thick as the hole depth should ideally be less than one third of the specimen thickness. The results were verified using a thin-plate correction provided by Stresscraft Ltd, and there were no significant changes in them[26]. To provide restraint against distortion and avoid introduction of bending induced stresses, a thick adhesive substrate was applied to the underside of the samples prior to drilling. In addition, the hole drilling results were compared to measurements on identical samples using at least one additional experimental method, to increase confidence in the measurements[26].

2.5 Fatigue testing

Fatigue tests were performed in tension-tension under load control using a servo-hydraulic test machine with a maximum capacity of 100 kN. Test frequency was 10 Hz and load ratio R was 0.1. The maximum nominal applied stress was 200 MPa. Test samples with LSP treatments C & D had strain gauges positioned on both faces 15 mm on either side of the scribe *i.e.* four gauges per sample. This was to monitor surface stresses for out-of-plane bending caused by peening induced distortion and to calculate the true local surface stress on each face. Fatigue tests were run until fracture and the total number of cycles until failure was recorded. Tests were performed on pristine 2024, on scribed 2024 without peening and on scribed 2024 with all four peening treatments. Two samples were tested in each configuration. After completion of the tests the fracture surfaces were examined optically and using a Scanning Electron Microscope (SEM).

3   Fatigue Life Prediction Model

The Abaqus software version 6.11 was used for FE analysis. Fatigue test specimens were modelled as a two-dimensional cross section as shown in Figure 3. Fatigue crack growth from the scribe root in the through thickness direction was modelled. For cracks growing in the through-thickness orientation the thickness of the sample was 80 mm and the width was 2 mm, and plane strain conditions were assumed. The fatigue test specimens are symmetrical about the scribe root and therefore symmetry boundary conditions were used with only half the geometry modelled. Elements of type CPE4R were used to mesh the geometry. The element size along the crack path was progressively increased from 0.1 µm at the scribe root to a maximum element size of 38 µm. Linear-elastic material properties were used with the material properties as per section 2.1. Crack advance was modelled using a node release scheme. The measured residual stress field was incorporated into the FE model as an initial condition using the Abaqus user subroutine Sigini. Since only a partial residual stress field was measured, a balancing section of residual stress had to be incorporated so that the input stress field was in a state of equilibrium. Therefore the modelled residual stress field along the crack path was as measured. The stress intensity factor (K) was calculated using the modified Virtual Crack Closure Technique (VCCT). Due to the high K_t values associated with the notches, the modelling assumption was that crack initiation occurred within a few cycles of the test start (i.e. no initiation period was considered) and that the initial fatigue crack length was that of the scribe depth.
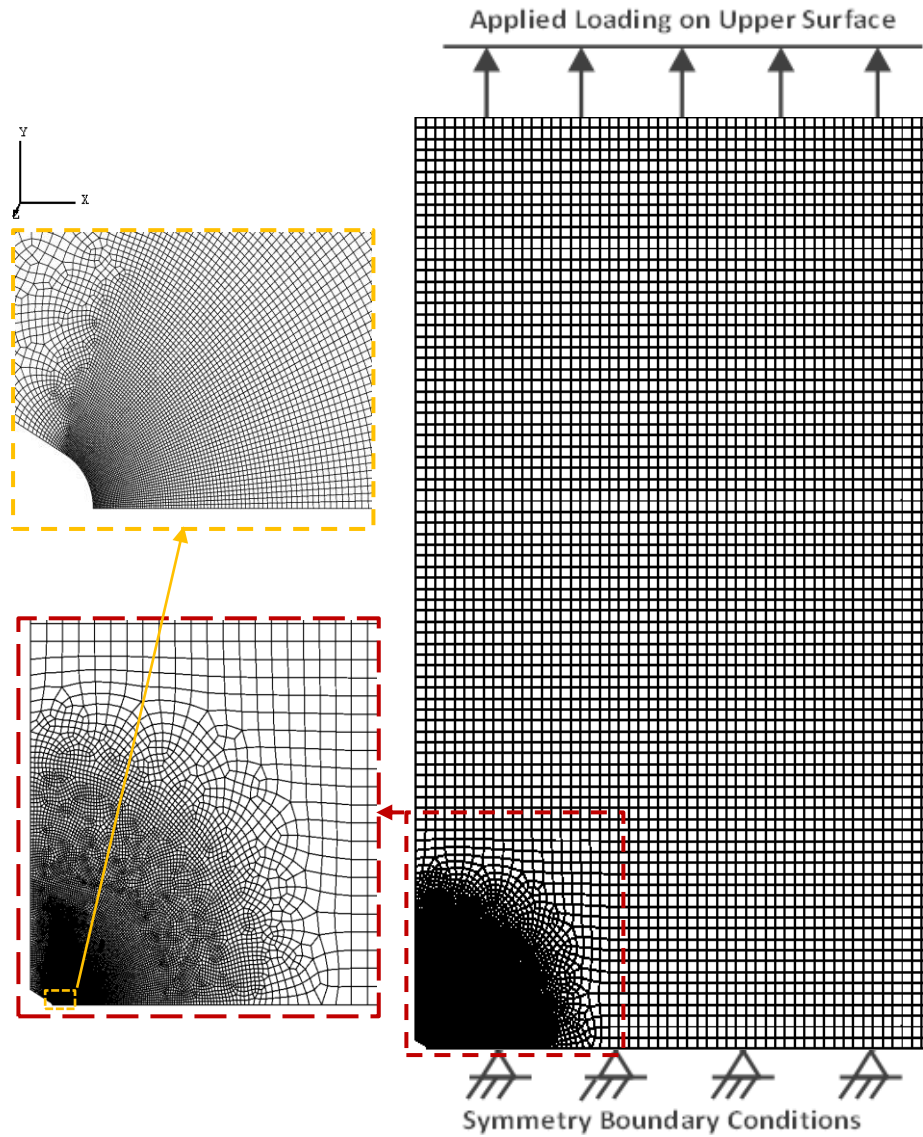
Figure 3: Finite element mesh used to model sample scribed to 50 μm

The effect on fatigue crack growth of the residual stress field was modelled using two approaches to calculation of ΔK_{eff}; namely modified superposition(M.SP) [27,28], and the Newman crack closure equation[29,30]. The modified superposition method is equivalent to the well-known superposition approach for $K_{tot,max}$ and when $K_{tot,min}$ is greater than zero. However the modified superposition method accounts for crack face contact by setting values of $K_{tot,min}$ less than zero as being equal to zero.

$$K_{tot,max} = K_{app,max} + K_{res} \quad (1)$$

$$K_{tot,min} = if\left(K_{app,min} + K_{res}\right)\begin{cases} \leq 0, & 0 \\ > 0, & K_{app,min} + K_{res} \end{cases} \quad (2)$$

To calculate fatigue lives the Walker fatigue crack growth equation was used to represent crack growth rates without residual stresses, where C and n are the Paris law material constants that define the fit and m determines the shift between stress ratios:

8

$$\frac{da}{dN} = C(\Delta K(1-R)^{m-1})^n \quad (3)$$

The material constants for 2024-T351 plate and sheet from the NASMAT material database[31] were used where C = 4.8 ×10^{-11}, n = 3.2 and m = 0.694.

The Newman equation uses a crack-closure-based approach to calculate an effective stress intensity factor range ΔK_{eff}. A crack opening stress ratio was calculated using equations below.

$$\frac{\sigma_{op}}{\sigma_{max}} = A_0 + A_1R + A_2R^2 + A_3R^3 \quad for \ R \geq 0 \quad (4)$$

$$\frac{\sigma_{op}}{\sigma_{max}} = A_0 + A_1R \quad for \ R < 0 \quad (5)$$

Where

$$A_0 = (0.825 - 0.34\alpha + 0.05\alpha^2)[cos(\pi\sigma_{max}/2\sigma_0)]^{1/\alpha} \quad (6)$$

$$A_1 = (0.415 - 0.071\alpha)\,\sigma_{max}/\sigma_0 \quad (7)$$

$$A_2 = 1 - A_0 - A_1 - A_3 \quad (8)$$

$$A_3 = 2A_0 + A_1 - 1 \quad (9)$$

According to Newman[30] for plane stress conditions α = 1 and for plane strain α = 3. In this work the α parameter was optimised to best predict the lives of baseline unpeened samples. An α of 3 was found as best fit. The α parameter was unchanged from baseline for the prediction of lives of peened samples.

The flow stress (σ_0) is defined as the average of yield stress and the ultimate tensile strength of the material. An effective SIF range (ΔK_{eff}) was then calculated using equation 10.

$$\Delta K_{eff} = \left[\frac{1 - \sigma_{op}/\sigma_{max}}{1 - R}\right]\Delta K_{app} \quad (10)$$

For the Newman crack closure approach, fatigue crack growth rate (FCGR) data[32] for 2024-T351 in the L-T direction at stress ratios of –2, –1, –0.5, 0, 0.5 and 0.7 (Figure 4 (A)) were used to calculate a master curve as shown in Figure 4 (B) below. The relationship between FCGR and ΔK_{eff} was characterised using the Paris relationship as shown in equation 11.

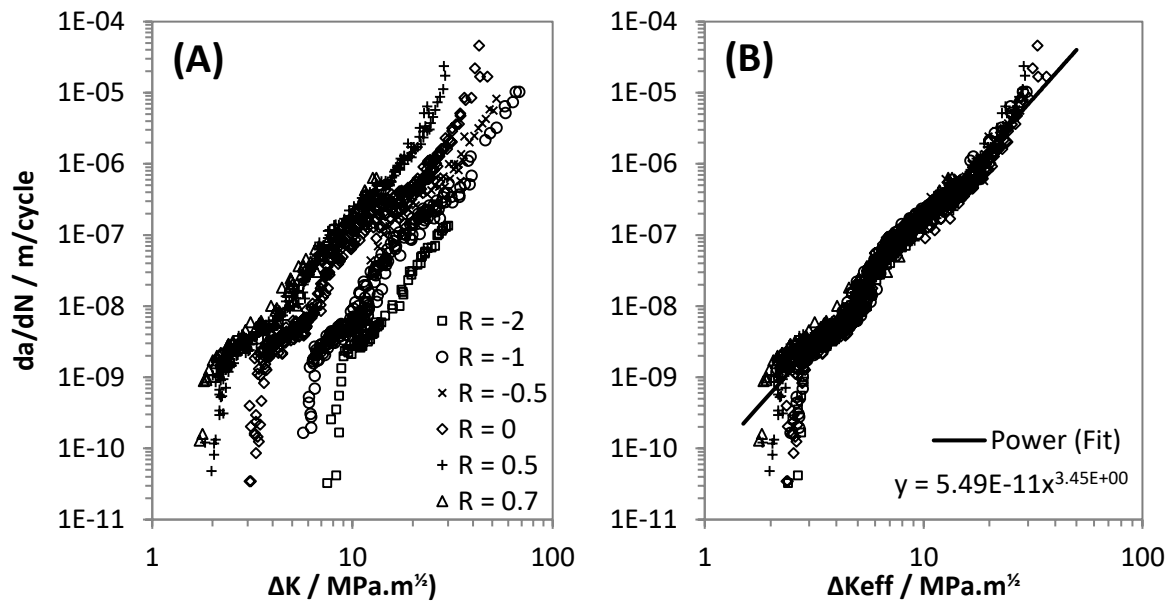$$\frac{da}{dN} = C\left(\Delta K_{eff}\right)^n \quad (11)$$

Figure 4: (A) FCGR data[32] and (B) material master curve ($\alpha = 3$) for 2024 T351.

4 Experimental Results

4.1 Sample distortion after laser shock peening

Since LSP was applied to one surface only, distortion of the test samples occurred to maintain equilibrium of the elastic stress field. This phenomenon is exploited for peen forming processes[33]. The distortion before and after peening was measured using a Coordinate Measurement Machine (CMM) and is shown in Figure 5. Untreated samples had some initial distortion present. This was augmented by the peening process.
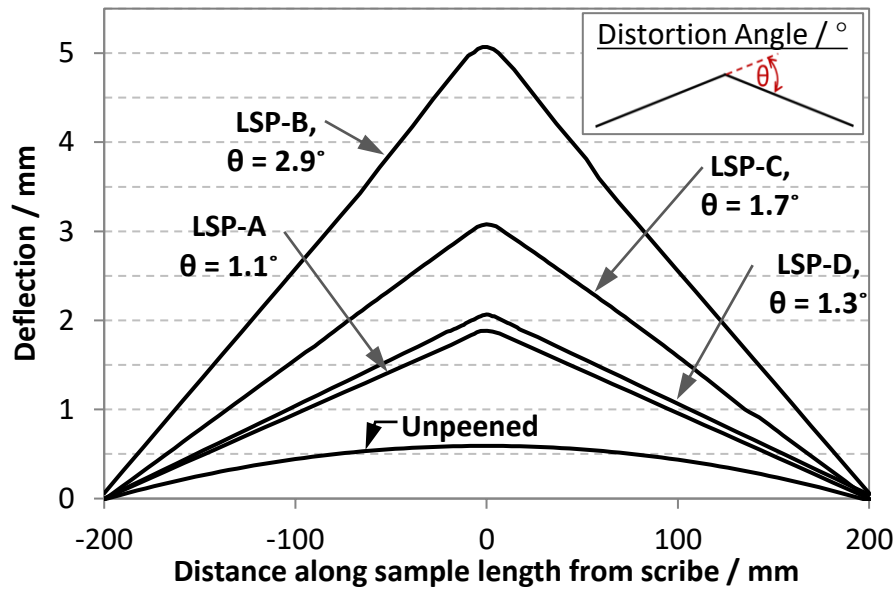
Figure 5: CMM measurement of distortion of peened surface after LSP treatment

The induced LSP distortion was confined to the peened area, and was locally of a constant radius of curvature. Outside the peened area, the ends of the sample followed the line of the deflected region at the edge of the peened area. A distortion angle was defined as the angle created by the material flanking the peened region, illustrated in Figure 5. The deflection of a sample was measured as the difference between the position of the sample ends and the position of the sample mid-point. Sample B has the largest deflection almost 3° and samples A and D the least (both 2°)

4.2 Measured residual stress fields

The residual stress fields measured in the σ_y direction (*i.e.* applied loading / crack opening direction) are shown in Figure 6. For detailed analysis of the residual stress fields, including measurements in the σ_x direction, please consult[26].

LSP treatments -A, -B and -C all induced tensile residual stress in the near surface (<100 µm depth). LSP-B resulted in greater near surface tensile stress than LSP-A, but also greater compression in depth noting that LSP-A and -B were nominally the same except LSP-B had a wider peened area. LSP-B produced the deepest compressive residual stress of all treatments studied, ≈0.8 mm.

The residual stress profile of LSP-C had tensile residual stress at the surface with a peak of 60 MPa at 40 µm depth. The near surface tensile residual stress extended 70 µm from the surface followed by a sub-surface compressive peak of −110 MPa at 0.1 mm depth. The residual stress then tended back towards tension and the depth of the compressive zone extended 0.7 mm from the peened surface

Compressive surface stress was obtained only by LSP-D treatment, which was approximately −70 MPa. It induced a sub-surface compressive peak greater than −200 MPa at 0.1 mm depth *i.e.* the most compressive peak stress compared to other treatments. The compressive stress extended 0.35 mm from the peened surface.
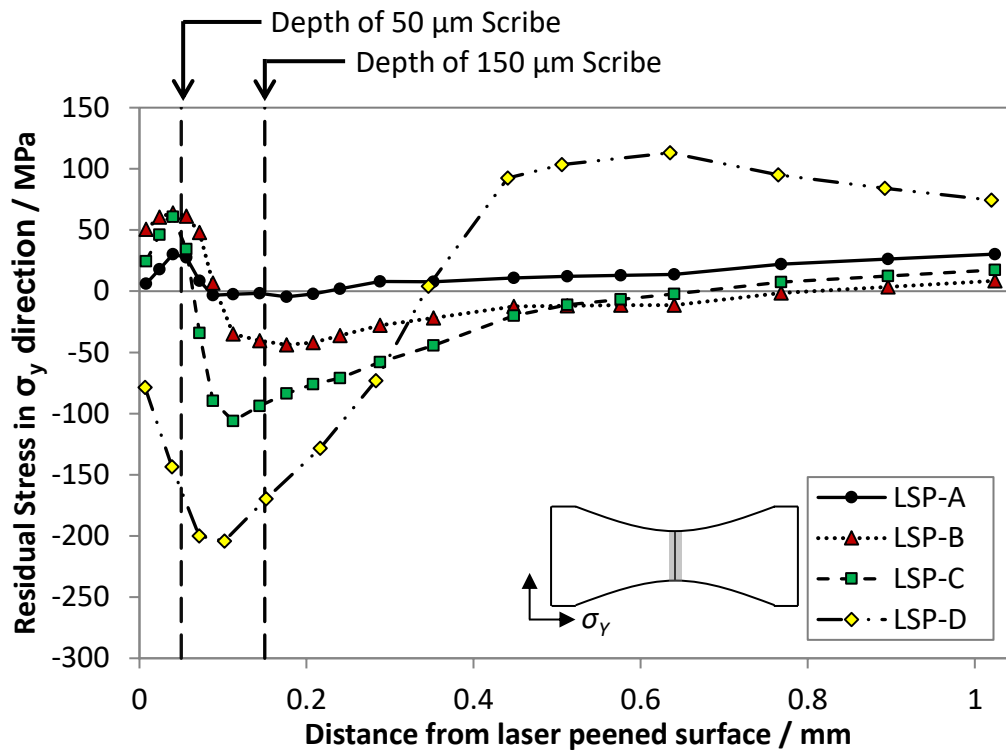
Figure 6: Profile of LSP induced residual stress fields measured in the σ_y direction.

4.3 Effect of sample distortion on test sample fatigue stress

Due to the distortion induced by LSP, the stresses imposed on the samples during testing were not uniaxial tension but were tension combined with out of plane bending. Surface strains 15 mm from the peen line were monitored throughout the fatigue loading cycle for LSP-C and LSP-D samples to measure the actual local stresses. Based on these measurements, calculated surface stresses adjacent to the peened region at maximum and minimum cyclic loads are shown in Figure 7. The distortion profile in the region of the peen patch had a constant radius of curvature; the remotely applied out of plane forces will give locally a pure bending condition, with constant surface stresses between the two strain gauge locations.

In samples peened with both LSP C and D treatments, stresses on the peened face were less than the nominal tensile stress and greater than nominal on the unpeened face. At maximum load the surface stresses in LSP C were 158 MPa and 242 MPa on the two faces, and at minimum load were –6 MPa and 46 MPa.

The LSP-D treatment resulted in less distortion than LSP-C and the effects on surface stress were not as great. On the peened face the maximum and minimum stresses were 186 MPa and 10 MPa and on the unpeened face they were 214 and 30 MPa.
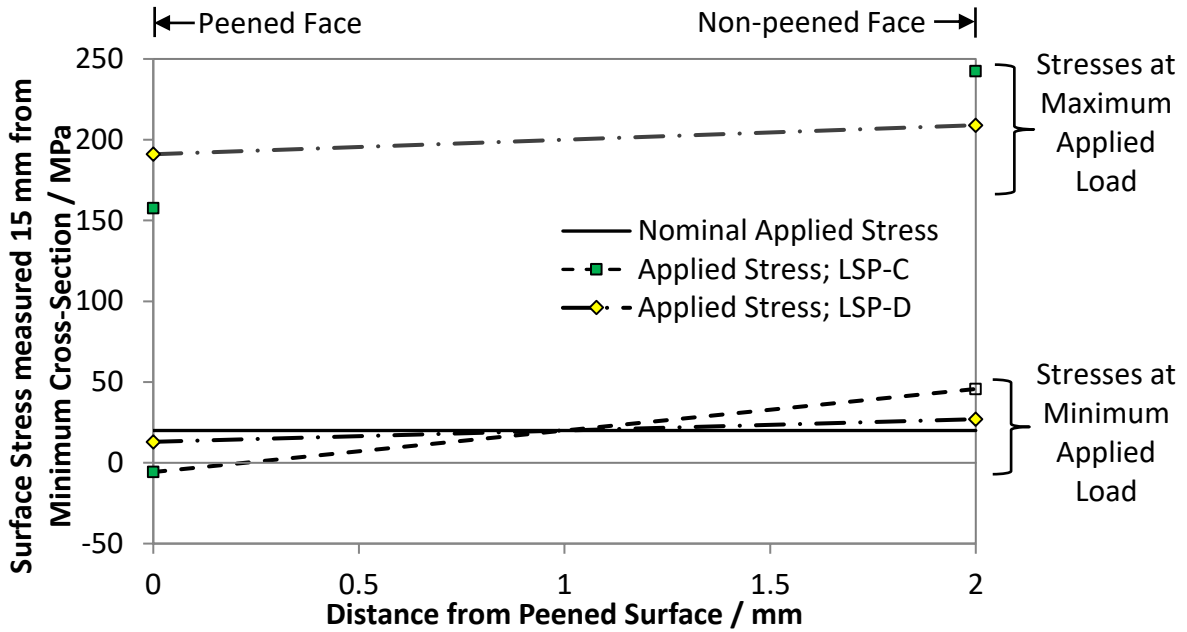
Figure 7: Measured bending surface stresses due to clamping peened samples LSP-C and -D during tension-tension fatigue loading.

4.4 Results of Fatigue Tests

The results of the fatigue tests are presented in Figure 8. For unpeened pristine and scribed samples, test data from the work of Cini[22]22 on the same 2024 2 mm batch, with identical sample geometry, tested under identical conditions are included. Figure 8a shows that without the beneficial effects of peening, the 50 μm and 150 μm scribes dramatically reduced the fatigue life from 4.2×10^5 cycles for pristine samples, to 7×10^4 cycles for 50 μm scribes, and to 2×10^4 for 150 μm scribes: factors of between 6 and 20. This life reduction has been reported in detail previously[22,23] and is a consequence of the high K_t of between 8 and 14 of the scribes.

Figure 8b shows that peening treatments changed fatigue life to different degrees. Peened sample lives are compared with the mean trend line of the unpeened samples. LSP-A treatment produced little or no change in fatigue life compared with untreated specimens. LSP-B treatment increased the fatigue life by factors of 1.5× and 1.8× for 50 μm and 150 μm scribes. After LSP-C treatment, an increase of fatigue life by 3.2× for the 50 μm and 3.4× for samples scribed to 150 μm was measured. The greatest improvement of fatigue life was after LSP-D where the fatigue life of 50 μm and 150 μm scribed samples increased by 3.3× and 13.3×. The improvements in life for LSPC with 50 μm scribe and for LSPD with both 50 and 150 μm scribes represent a minimum value of life as these samples failed from cracks remote from the scribes. Had remote failure not intervened, the lives of the peened scribe features would be greater still.
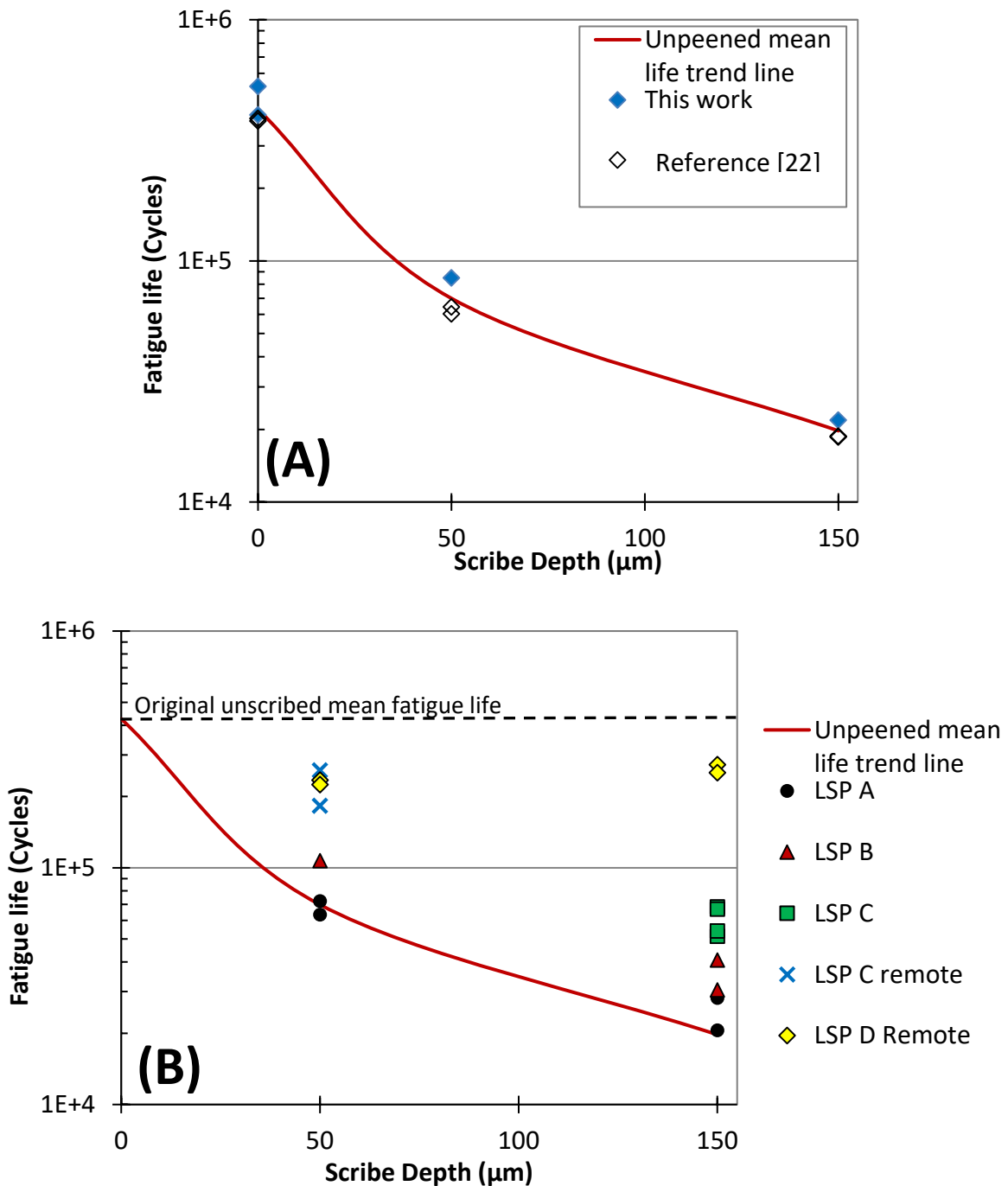
Figure 8: (A) Fatigue lives of unpeened samples showing the reduction in fatigue lives produced by scribes of 50 and 150 µm and (B) Fatigue lives plotted against scribe depth for the 4 peening treatments showing increases in fatigue life relative to the unpeened trend line. Data points marked C & D remote failed remote from the scribe line even though fatigue cracks initiated there.

4.5 Fractography

Samples scribed treated with LSP-A and LSP-B exhibited similar fracture characteristics. A representative illustration of the fracture surfaces is shown in Figure 9. Two types of fatigue crack propagation process were observed. The first initiated at the root of the scribe and propagated in the

through thickness direction. In samples scribed to 50 μm depth the crack had propagated 40-70 μm at fracture. In samples scribed to 150 μm depth cracks had propagated approximately 140-160 μm. The second type of crack initiated at the interface between the scribe runout and sample edge and propagated in the sample width direction. The length of these cracks at fracture was approximately 10-15mm in samples scribed to 50 μm depth and 5-10 mm in samples scribed to 150 μm depth. This is a preferred site of initiation in peened samples due to reduced residual stress and an enhanced K_t at the sample edge.
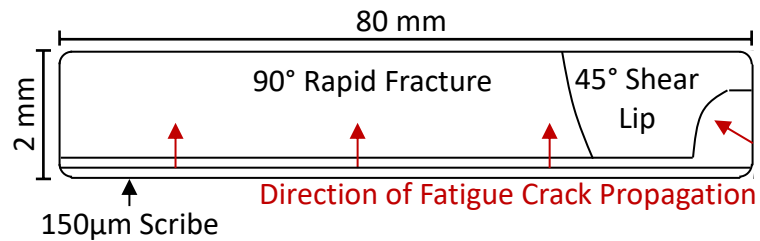

Figure 9: Illustration of representative fatigue fracture surface for peening treatments A, B, C.

Similar behaviour was observed in samples with 150 μm scribe treated with LSP C. (Figure 9). Samples with 50 μm scribes treated with LSP-C did not fail at the scribe. However a fatigue crack was observed in the SEM to have initiated at the root of the scribe as shown in Figure 10. The actual failure location was approximately 2mm from the scribe line a within the peened region.
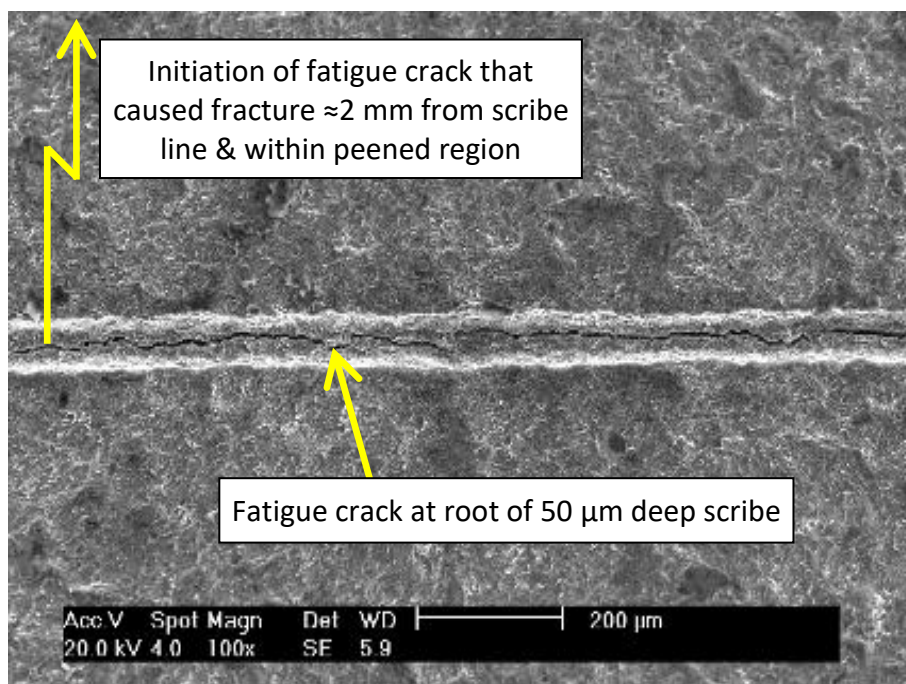

Figure 10: SEM picture of fatigue crack at root of 50 μm scribe with LSP-C peening; final fracture occurred remote from scribe

All samples treated using LSP-D failed due to fatigue cracks initiating on the unpeened face remote from the scribe. As in peening treatment C, Initiated fatigue cracks were observed at the root of both

50 μm and 150 μm scribes. The actual failure location was approximately 4 mm from the scribe line and located outside the peened region.

5   Comparison of Predicted and Measured Fatigue Lives

Residual stress intensity factors (K_{res}) for cracks growing from the roots of 50 μm and 150 μm scribes are shown in Figure 11 plotted as a function of distance from the peened surface. K_{res} values associated with LSP-A are positive (tensile) for all crack lengths. This was due to the tensile residual stress at the surface (Figure 6). The residual stress fields of LSP-B and -C gave a K_{res} that was initially positive at the 50 μm scribe root, becoming negative at a crack tip located approximately 165 μm and 85 μm from the peened surface. K_{res} associated with cracks after LSP-D treatment was negative at all crack lengths.
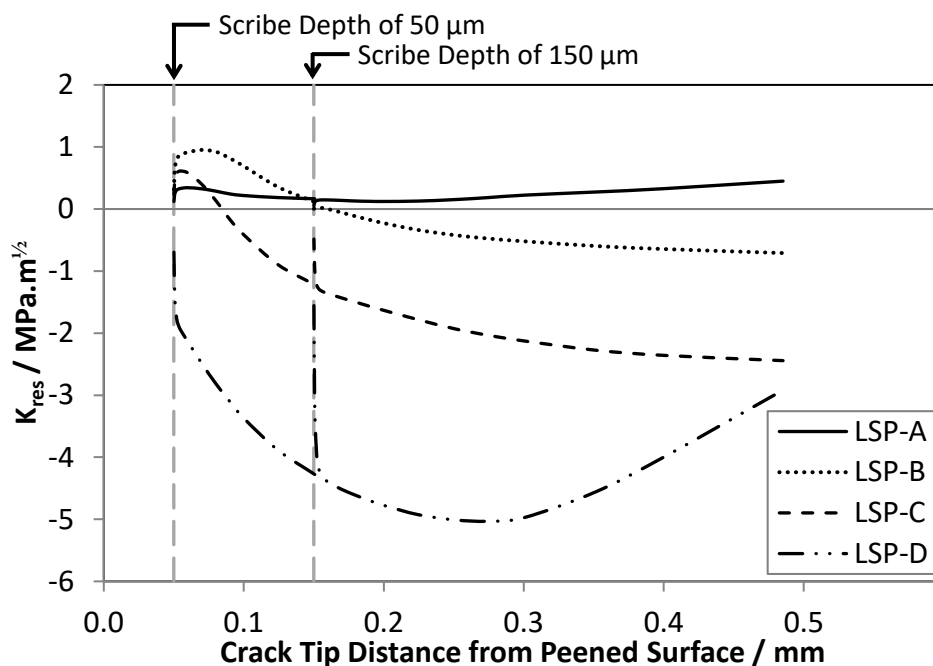

Figure 11: Comparison of calculated residual stress intensity factors plotted against crack depth.

The effect of K_{res} on the effective stress intensity range ΔK_{eff} and stress ratio R_{eff} was determined using the modified superposition and the Newman equation approaches described in section 3. The results are shown in Figure 12 and Figure 13. Considering LSP-A, since K_{res} was positive, ΔK_{eff} will be identical to ΔK_{app} and the effect of peening on crack growth life will be due to the slight increase in tensile R ratio R_{eff}. Although K_{res} in samples peened with LSP-B became negative at crack depths >150 μm, it was not sufficiently negative to reduce K_{min} below zero, and so there was no effect on ΔK_{eff} and again the effect of peening on life will be due to R_{eff} changes only. The residual stress induced by LSP-C and -D treatments was great enough to reduce both ΔK_{eff} and R_{eff} as shown in Figure 12. These changes will have a significant effect on crack growth rates and life.

Figure 13 shows ΔK_{eff} values predicted by the Newman closure model. This predicts that LSP-A actually will increase ΔK_{eff} and R_{eff} as the tensile residual stress reduces the K_{op} value. All other

16

peening treatments reduce ΔK_{eff} and R_{eff} once the crack tip had propagated through any near-surface tensile stress field.
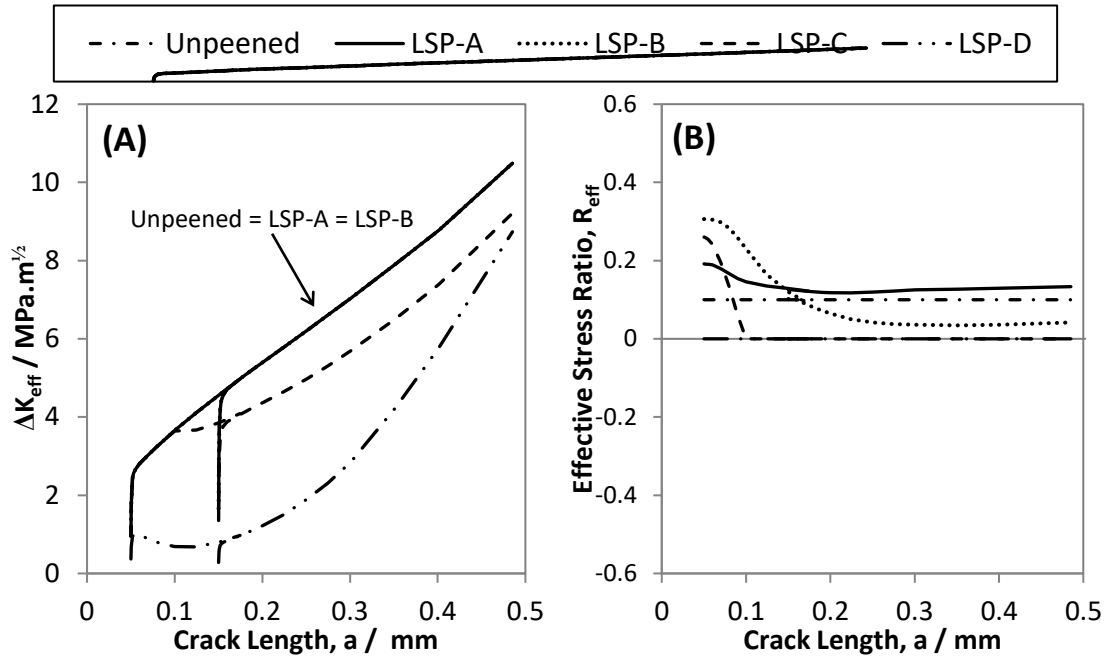
Figure 12: (A) Effective Stress intensity factor range and (B) stress ratio calculated using the modified superposition method plotted against crack depth.
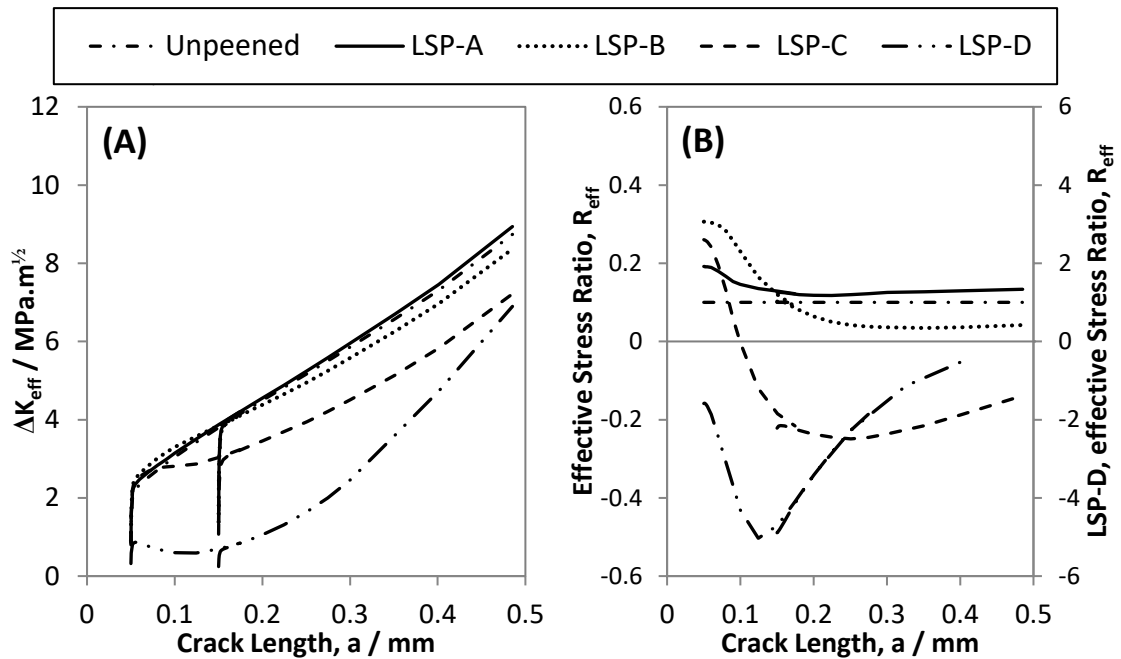

Figure 13: (A) Effective stress intensity factor range and (B) Effective stress ratio calculated using the Newman crack closure approach plotted against crack depth

Using this data predictions of fatigue life were made by comparing the predicted a Vs N curve to experimental measured failure crack lengths as illustrated in Figure 14 using unpeened and LSP-C samples as an example.
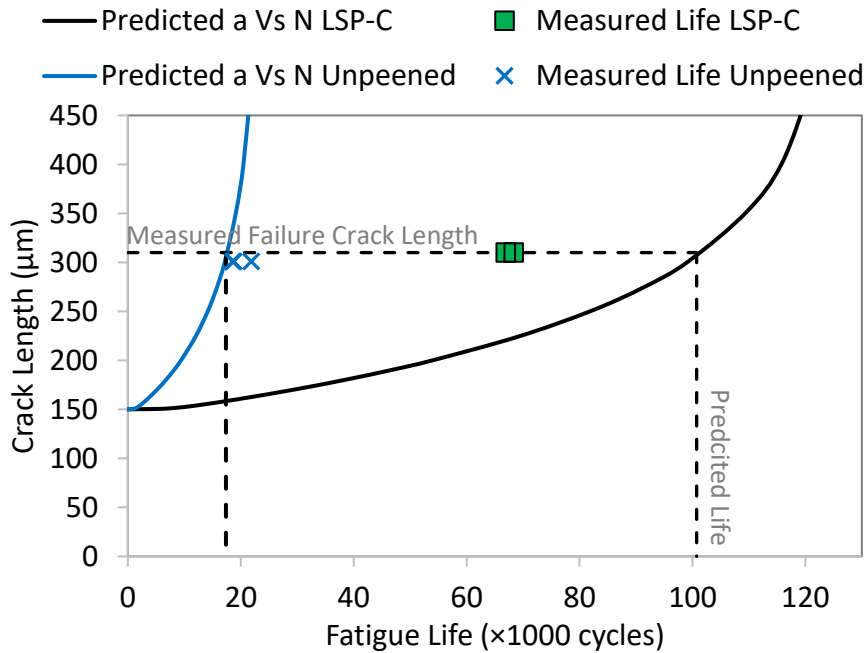
Figure 14: Predicted crack length vs. cycles for unpeened and LSP-C samples scribed to 150 μm depth

Figure 15 shows predicted fatigue lives by modified superposition and by Newman crack closure plotted against mean experimental lives for all samples. The continuous line represents perfect correlation between experimental and predicted lives. Agreement between predicted and experimental lives for all samples which failed from the scribes was within a factor of 2, with predicted crack growth lives shorter than experimental ones, suggesting there was an initiation life prior to crack development. Predictions of the Newman equation were consistently more accurate than modified superposition but the difference was small. Samples which failed at locations remote from the scribe had experimental lives consistently between 2 and 3×10^5 cycles, and predictions based on crack growth from scribes will not accurately reflect experimental life. In the case of peening treatment D, predicted lives were significantly greater than those measured experimentally for remote initiation. SEM observations of cracking at the scribe root in these samples indicated that cracks had initiated at the scribe roots; the absence of failure from the scribe locations was not because of inhibition of initiation; instead the predicted life was significantly longer than the life to initiate and grow cracks to failure from remote locations at the free surface (2.4-2.6 $\times 10^5$ cycles). In the case of peening treatment C applied to a 50 μm defect, Figure 10 shows initiation from the scribe root in this sample as well. The actual life was almost the same (2.2 $\times 10^5$ cycles for remote initiation). In this case the predicted life was smaller than the experimental one, following the same trend as predictions for LSP A and B.
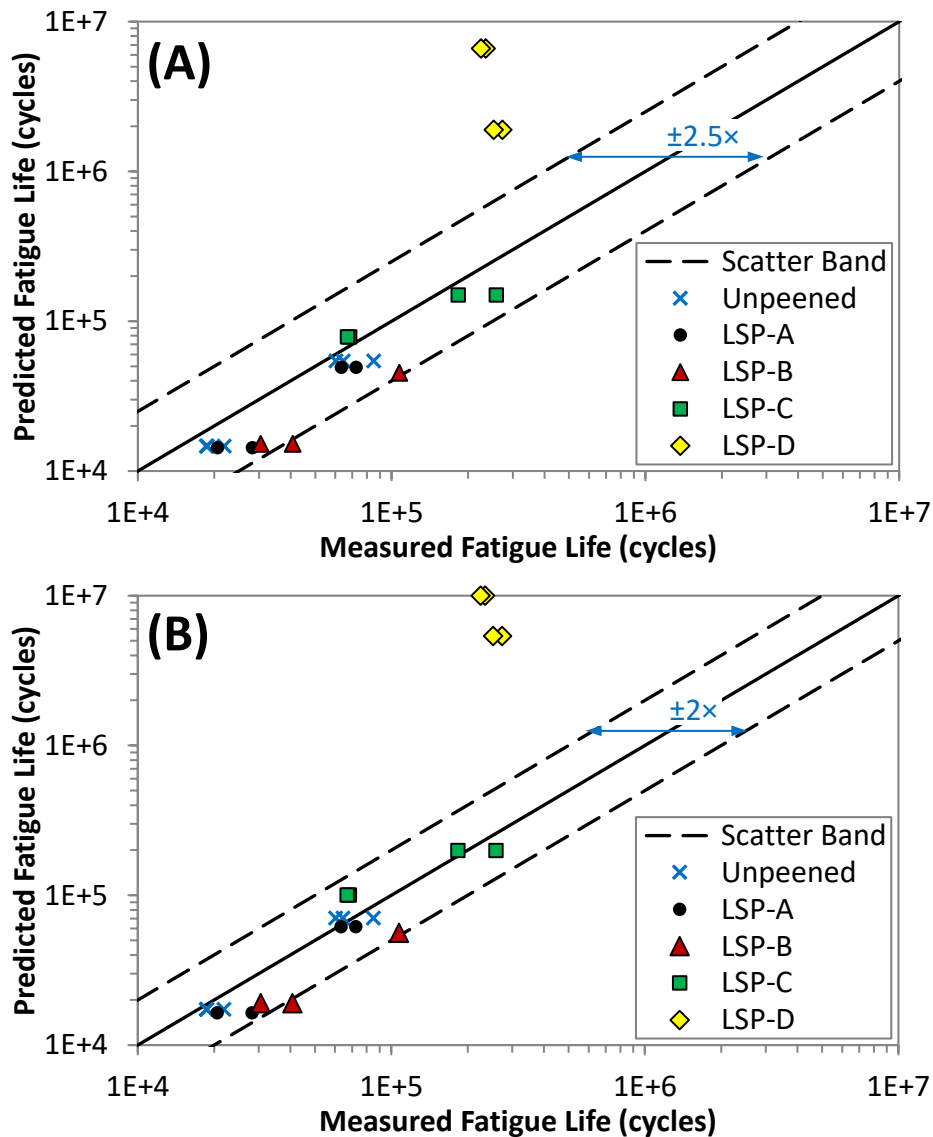
Figure 15: Comparison of experimental and predicted fatigue lives using (A) modified superposition and (B) Newman closure approach.

6   Discussion

6.1   Effect of laser shock peening parameters on the residual stress field

Samples treated with LSP-A, -B and -C all had tensile residual stress at the surface. Surface tensile residual stresses have been attributed to reflection of pressure pulse shock waves from the sample back surface, and/or reverse yielding because of relaxation of the stored elastic strain in the subsurface material[33, 34]. Long pulse durations have been reported to result in tensile residual stress at or near the surface[34-36], whereas the surface stress was in compression for samples treated with LSP-D. This is consistent with the pulse duration used in this work of 18 ns for LSP-A and -B, and 8 ns for LSP-D.

6.2   Development of model to predict fatigue life recovery

The large elastic K_t values of 8 and 14 for the 50 μm and 150 μm deep scribes suggest that fatigue crack initiation in unpeened samples will occur within a few cycles of the start of fatigue cycling, and almost the entire life; (reduced to only 10% of pristine sample life) is therefore consumed by crack growth from the notch root to a failure crack length, with propagation in the L-S and L-T directions. A predictive model based on crack growth is therefore appropriate. Ideally, master curve crack growth data for short cracks propagating in the L-S direction in 2 mm 2024 sheet is required as input, but is not known to exist. In the case of crack growth from the 50 μm scribe, the first 10-20 μm of growth will be through clad layer material, a relatively pure aluminium with reduced strength and increased ductility compared with the substrate. Comparison of crack growth rates in 7XXX and 2XXX aluminium alloys suggests that increased ductility will reduce crack growth rates over the 10-20 μm increment. Figure 16a shows ΔK_{eff} at this length is between 2.5-3.0 MPa m$^{1/2}$, and figure 4 shows the da/dN values to be 2-3 X10^{-9} m/cycle. Approximately 10^4 cycles would then be required to grow 20 μm using available long crack data.   No relevant short crack growth data is known for pure cladding, and it is perhaps unwise to attempt to quantify the error further. Long crack L-T data[32] applied in both Newman and superposition models give good agreement with experiment as Figure 15 shows, for both unpeened and peened conditions.

Experimental measured crack lengths at the termination of crack growth from the scribes were used in the calculations rather than predicted failure crack lengths at $K_{max} = K_c$, due to the complicated fatigue behaviour observed on experimental fracture surfaces. The modelling assumption was that fatigue cracks would initiate at the scribes and propagate in the through thickness direction. This was observed in the experiments. Fatigue cracks also initiated at the ends of the scribes and propagated in the sample width direction. These cracks terminated the test at the condition of $K_{max} = K_c$. It was not the aim of this paper to accurately model such a complicated fatigue process but rather predict the effect of residual stress on fatigue crack propagation from the scribes. Therefore the final crack length used was the measured crack length at which crack growth from the scribes terminated.

6.3   Effect of residual stress field on crack growth life

The effect of the different laser treatments on fatigue life ranged from a factor of 13.3 increase to a 0.97 decrease. This variation in response may be attributed to the size, position and depth of the residual stress field. The residual stress field determines the K_{res} value and how it changes with crack depth. Externally applied loads interact with sample distortion to determine externally applied K_{max} and K_{min} values; these are then modified by K_{res} to determine ΔK_{eff} which in turn determines crack growth life. The observation in 4.5 that cracks initiate at both 50 μm and 150 μm deep scribes even though the specimens ultimately failed elsewhere, indicates that initiation from these defects with K_t values of 8 and 14 occurred quickly. Whether the samples fail via crack growth from the scribe will depend on whether crack growth life after initiation is greater or smaller than the total fatigue life of the sample material remote from the scribe.

Figure 6 shows there are significant differences between the treatments in whether there is tension residual stress at the surface (treatments A, B and C, not for D), and its size and depth (75 MPa for LSP-B and extending up to 0.1 mm below the surface).

These differences translate into the different relations between K_{res} and crack depth shown in Figure 11. The effect of the surface residual tensile field is to create positive values of K_{res} which enhance da/dN values and decrease fatigue life. LSP-A maintains positive K_{res} values throughout the entire depth; LSP-B and -C move into negative values of K_{res} at depths of 150 μm and 90 μm respectively. Overall lives of -B and -C will be determined by the balance between mild acceleration caused by the positive K_{res} and the retardation caused by the region of negative values. LSP treatment -D has negative K_{res} throughout as well as the largest negative K_{res} value, and all stages of growth will be subject to retardation.

Figure 12 and Figure 13 show that there are considerable differences in ΔK_{eff} values produced by the different peening treatments. There is little difference in the calculated values of ΔK and ΔK_{eff} produced by the two models. ΔK values for the unpeened sample are also shown on these figures. There is little or no difference between calculated ΔK_{eff} values for peening treatments A and B and the unpeened sample. K_{res} will influence mean K and therefore R values, rather than ΔK. Differences in R_{eff} can be seen in Figure 12 and Figure 13 but small changes in positive tensile R ratio will not have a big effect on growth rates. When K_{res} is negative and is sufficiently big to make the R ratio negative with $K_{min} < K_{cl}$ (below the closure point), the decrease in ΔK_{eff} will have a powerful effect in reducing crack growth rates. This situation applies for treatments LSP-C and -D.

Treatment C, although tensile at the surface, has sufficient subsurface compressive residual stress to reduce ΔK_{eff} significantly, with consequent reduction in da/dN and increases in life. LSP-D has the smallest values of ΔK_{eff}: the smallest calculated value is <1 MPa m$^{1/2}$, less than ΔK_{th}, the long-crack threshold for growth. An infinite fatigue life for the peened region might be expected; however failure elsewhere intervenes, giving a mean finite sample life of 2.4 X 10^5 cycles. This is less than the original mean life of 4 X 10^5 cycles, because the distortion induced surface bending stress is greater than the original tensile one.

7   Conclusions

1. For thin section aluminium, small diameter laser spots (0.4-1.5 mm), low energy per pulse (0.02-2.8 J), with high levels of overlap, produced greatest compressive residual stress, closest to equibiaxiality with minimum sample distortion.
2. Distortion severity was dependent on laser process parameters. The distortion promotes out-of-plane bending, modifying the nominal in-plane stresses in fatigue loading by up to 20% and reducing the apparent fatigue life of the unpeened surface.
3. Surface scribes 50 μm and 150 μm deep reduce the fatigue life of 2024 aluminium sheet to only 5% of the pristine material. Laser peening of the scribed area increases fatigue life by reducing fatigue crack growth rates to an extent dependent on the residual stress field. Initiation of cracks at scribe roots was not inhibited by peening.

4. Fatigue life recovery was limited to 61% of the life of the pristine material, as a consequence of competing sites for crack initiation on the unpeened sample surface, subjected to distortion-induced enhanced surface stresses.

5. Models of the effect of residual stress fields based on K_{res} and crack closure concepts conservatively predicted the effects of different peening treatments on recovered fatigue life.

8 Acknowledgements

9 References

1. Sticchi M, Schnubel D, Kashaev N. Review of residual stress modification techniques for extending the fatigue life of metallic aircraft components. *App Mech Reviews* 2015; 67: 010801-1-9.

2. Ivetic G, Meneghin I, Troiani E, Molinari G, Ocaña JL, Morales M, Porro J, Lanciotti A, Ristori V, Polese C, Plaisier J, Lausi A. Fatigue in laser shock peened open-hole thin aluminium specimens. *Mater Sci and Engng* A. 2012; 534: 573-579.

3. Dorman M, Toparli MB, Smyth N, Cini A, Fitzpatrick ME, Irving PE. Effect of laser shock peening on residual stress and fatigue life of clad 2024 aluminium sheet containing scribe defects. *Mater Sci Engng A*. 2012: 548: 142-151.

4. Chahardehi A, Brennan FP, Steuwer A. The effect of residual stresses arising from laser shock peening on fatigue crack growth. *Engng Fracture Mech.* 2010; 77, no. 11: 2033-2039.

5. Maawad E, Sano Y, Wagner L, Brokmeier H, Genzel C. Investigation of laser shock peening effects on residual stress state and fatigue performance of titanium alloys. *Mater Science and Engng A.* 2012; 536: 82-91.

6. Rodopoulos CA, Romero JS, Curtis SA, De los Rios ER, Peyre P. Effect of controlled shot peening and laser shock peening on the fatigue performance of 2024-T351 aluminium alloy. *J Mater Engng and Performance.* 2003; 12, no. 4: 414-419.

7. Toparli MB, Fitzpatrick ME. Residual stresses induced by laser peening of thin aluminium plates. 2011; in Scardi P, Azanza Ricardo CL. eds. 8th European Conference on Residual Stresses, Trento, Italy, 26-28 June 2010, *Materials Science Forum*; 681: 504-509.

8. Sano Y, Masaki K, Gushi T, Sano T. Improvement in fatigue performance of friction stir welded A6061-T6 aluminium alloy by laser peening without coating. *Mater and Design.* 2012: 36: 809-814.

9. Salvati E, Lunt AJG, Ying S, Sui S, Zhang HJ, Heason C, Baxter G, Korsunsky AM. Eigenstrain reconstruction of residual strains in an additively manufactured shot peened nickel superalloy compressor blade. *Comput Methods Appl Mech Engrg* 2017; 320; 335-351.

10. DeWald AT, Hill MR. Eigenstrain based model for prediction of laser peening residual stresses in arbitrary three dimensional bodies part 2: Model verification. *J Strain Anal Eng Des* 2009; 44(1); 13-27.

11. Ding K, Ye L. *Laser Shock Peening: Performance and Process Simulation*, Woodhead; Cambridge 2006.

12. Ivetic G. Three-dimensional FEM analysis of laser shock peening of aluminium alloy 2024-T351 thin sheets. *Surface Engineering*, 2011; 27, no. 6: 445-453.

13. Jiang YF, Fang L, Li Z, Tang Z. Effects of sheet thickness on residual stress distribution by laser shock processing of 7050-T7451 aluminium alloy. *Advanced Materials Research*. 2011; vol. 189-193: 3778-3781.

14. Sticchi M, Staron P, Sano Y, Meixer M, Klaus M, Rebelo-Kornmeier, Huber N, Kashaev N. *J Eng*. 2015; 13: 97-105.

15. Huang S, Zhou JZ, Sheng J, Lu JZ, Sun GF, Meng XK, Zuo LD, Ruan HY. *Eng Frac Mech*. 2013; 99: 87-100.

16. Correa C, Peral D, Porro JA, Diaz M, Ruiz de Lara L, Garcia-Beltran A. *Optics Laser Tech* 2015; 73; 179-187.

17. Achintha M, Nowell D, Furfari D, Sackett EE, Bache MR. Fatigue life behaviour of geometric features subjected to laser shock peening; Experiments and modelling. *Int J Fat*. 2014, 62: 171-179.

18. Kashaev N, Ventzke V, Horstmann M, Chupakhin S, Riekehr S, Falk R, Maawad E, Staron P, Schell N, Huber N. *Inter J Fatigue*. 2017; 98: 223-233.

19. Luo S, Nia X, Zhou L, Li Y, He W. *ASM International*. 2018; 27(3): 1466-1474.

20. Fleury, RMN, Nowell D. Evaluating the influence of residual stresses and surface damage on fatigue life of Nickle base superalloys, *Int J Fatigue* 2017; 105: 27-33.

21. Zhan Z, Hu W, Shen F, Meng Q, Pu J. Guan Z. Fatigue life calculation for a specimen with an impact pit considering impact damage residual stresses and elastic-plastic fatigue damage *Int J Fatigue*. 2017, 96: 208-223.

22. Cini A, Irving PE. Development of fatigue cracks from mechanically machined scratches on 2024 T351 Aluminium alloy Part I Experiments. *Fatigue Fract Eng Mater Struct.* 2017; 40: 776-789.

23. Cini A. *Scribe marks at fuselage joints: initiation and propagation of fatigue cracks from mechanical defects in aluminium alloys*. Ph D thesis , Cranfield University; 2012.

24. Grant PV, Lord JD, Whitehead PS. *Measurement good practice guide no. 53: the measurement of residual stresses by the incremental hole drilling technique*. National Physical Laboratory; Teddington, UK; 2002.

25. Schajer GS. Measurement of non-uniform residual stresses using the hole-drilling method. Part I. Stress calculation procedures. *J Eng Mater Technology*. 1988; 110, no. 4: 338-343.

26. Toparli MB. *Analysis of residual stress fields in aerospace materials after laser peening*. PhD thesis. The Open University; 2012.

27. Ma YE, Staron P, Fischer T, Irving PE. Size effects on residual stress and fatigue crack growth in friction stir welded 2195-T8 aluminium – part II modelling. *Int J Fatigue*. 2011; 33: 1426-1434.

28. Fratini L, Pasta S, Reynolds AP, Fatigue crack growth in 2024-T351 friction stir welded joints longitudinal residual stress and microstructure effects. *Int J Fatigue.* 2009; 31: 495-500.

29. LaRue JE, Daniewicz SR. Predicting the effect of residual stress on fatigue crack growth. *Int J fatigue.* 2007; 29: 508-515.

30. Newman JC. A crack opening equation for fatigue crack growth. *Int J Fracture.* 1984; 24: 131-135.

31. https://www.swri.org/consortia/nasgrow.

32. NASGRO Fracture Mechanics and Fatigue Crack Growth Analysis Software, Version 4.02, NASA-JSC and SwRI, September 2002.

33. Hu Y, Xu X, Yao Z, Hu J. Laser peen forming induced two way bending of thin sheet metals and its mechanisms. *J Applied Physics*. 2010; 108, no. 7:

34. Clauer AH, Lahrman DF. Laser shock processing as a surface enhancement process. *Key Eng Mat*. 2001; 197: 121-142.

35. Zhang W, Yao YL. Micro scale laser shock processing of metallic components. *J Manufacturing Sci Eng.* 2002; 124, no. 2: 369-378.

36. Akita K, Kuroda M, Withers PJ. Dynamic analysis of residual stress introduced by laser peening. *Mater Sci Forum.* 2006; 524-525: 135-140.